

CONDENSED  
MATTER

# Magnetic Memory Effect in Planar Ferromagnet/Superconductor/Ferromagnet Microbridges Based on Highly Diluted PdFe Alloy

L. N. Karelina<sup>a, \*</sup>, N. S. Shuravin<sup>a</sup>, A. S. Ionin<sup>a, b</sup>, S. V. Bakurskiy<sup>c</sup>, S. V. Egorov<sup>a, d</sup>,  
I. A. Golovchanskiy<sup>b, e</sup>, V. I. Chichkov<sup>e</sup>, V. V. Bol'ginov<sup>a</sup>, and V. V. Ryazanov<sup>a, b, e</sup>

<sup>a</sup> Institute of Solid State Physics, Russian Academy of Sciences, Chernogolovka, Moscow region, 142432 Russia

<sup>b</sup> Moscow Institute of Physics and Technology (National Research University),  
Dolgoprudnyi, Moscow region, 141700 Russia

<sup>c</sup> Skobeltsyn Institute of Nuclear Physics, Moscow State University, Moscow, 119991 Russia

<sup>d</sup> Russian Quantum Center, Skolkovo, Moscow, 143025 Russia

<sup>e</sup> National University of Science and Technology MISiS, Moscow, 119049 Russia

\*e-mail: lkarelina@issp.ac.ru

Received May 6, 2022; revised June 2, 2022; accepted June 2, 2022

The magnetoresistance of a planar microbridge based on a three layer Pd<sub>0.99</sub>Fe<sub>0.01</sub>–Nb–Pd<sub>0.99</sub>Fe<sub>0.01</sub> FSF sandwich near its superconducting transition is studied. We previously showed that the magnetoresistance curve of such samples is hysteretic and contains dips (negative peaks of the resistance) in the coercive fields. In this work, it is found that the low-resistance state has a memory effect. Functioning of such a sample as a superconducting memory element is demonstrated. The effect of the ferromagnetic Pd<sub>0.99</sub>Fe<sub>0.01</sub> layer on the superconducting transition temperature of the proposed memory element is studied by measuring the dependence of the critical temperature of bilayer Pd<sub>0.99</sub>Fe<sub>0.01</sub>–Nb FS structures on the thickness of the Pd<sub>0.99</sub>Fe<sub>0.01</sub> layer.

DOI: 10.1134/S0021364022601105

Layered ferromagnet–superconductor (FS) hybrid structures are very promising for developing memory elements for superconducting logic (see, e.g., [1, 2] and references therein). Unusual properties of FS hybrids are due to the spin antagonism of superconductivity and ferromagnetism leading to a number of peculiar phenomena. In particular, the dependence of the critical temperature  $T_c$  of FS structures on the thickness of the F layer can be nonmonotonic [3] or even reentrant [4, 5]. Similar dependences were observed in FSF structures (see, e.g., [6]), as well as in structures of a larger number of periodically alternating F and S layers [7–11]. If a layered FS structure contains several ferromagnetic layers, its critical temperature can differ for parallel and antiparallel orientations of their magnetizations [10–14]. This allows the implementation of “spin-valve effects” (see review [15]). The use of strong ferromagnets or half-metals with high spin polarization makes it possible to significantly change the critical temperature of such samples due to spin-triplet superconducting correlations (see review [16]). The maximum change in the critical temperature caused by the spin-valve effect was 1.6 K [17, 18].

Our group studies the opposite limit of extremely weak ferromagnets based on a dilute Pd<sub>0.99</sub>Fe<sub>0.01</sub> alloy. A low exchange energy in the F layer and planar magnetic anisotropy allowed the implementation of Josephson magnetic memory elements based on Nb–Pd<sub>0.99</sub>Fe<sub>0.01</sub>–Nb SFS sandwiches [2, 19–21], which are technologically and frequency compatible with superconducting rapid single-flux quantum (RSFQ) logic [22]. In [2, 23], the possibility of miniaturization of the proposed elements by using rectangular SISFS (superconductor–insulator–thin superconducting spacer–ferromagnet–superconductor) Josephson junctions was studied. It was shown that the area reduction for a Josephson memory element based on a Pd<sub>0.99</sub>Fe<sub>0.01</sub> alloy is limited to about 2 μm<sup>2</sup> [2]. The fundamental origin of the emerging limitation is related to using the dependence of the critical current of the SFS sandwich on the magnetization flux through the cross section of the Pd<sub>0.99</sub>Fe<sub>0.01</sub> layer for encoding the digital state. Further miniaturization can be achieved by using planar FSF microbridges, where the critical current and resistance depend on the magnitude and mutual orientation of the magnetizations of F layers (see, e.g., review [24]). Our previous study

[1] of the magnetoresistance of rectangular  $\text{Pd}_{0.99}\text{Fe}_{0.01}\text{-Nb-Pd}_{0.99}\text{Fe}_{0.01}$  microbridges with planar sizes of 5–100  $\mu\text{m}$  at temperatures within the superconducting transition already revealed a noticeable magnetoresistance effect. The effect is manifested in hysteresis magnetoresistance dips (negative, low-resistance peaks), which are most clearly observed in the smallest microbridges (5–20  $\mu\text{m}$ ). In this work, we demonstrate that the low-resistance state has a memory effect, and therefore,  $\text{Pd}_{0.99}\text{Fe}_{0.01}\text{-Nb-Pd}_{0.99}\text{Fe}_{0.01}$  FSF microbridges can be used as superconducting logic elements.

The main object of the study is a  $6 \times 20\text{-}\mu\text{m}$  planar  $\text{Pd}_{0.99}\text{Fe}_{0.01}\text{-Nb-Pd}_{0.99}\text{Fe}_{0.01}$  FSF microbridge placed between the superconducting niobium pads (Fig. 1a). The fabrication technology is described in detail in [1]. The thicknesses of the upper and lower F layers are 45 and 22 nm, respectively, and the thickness of the superconducting layer is 13 nm. The coercive field of the upper F layer is 2–3 times larger than that of the lower one [25], which makes it possible to implement the superconducting spin valve proposed in [12, 13]. The measurements were carried out in a  $^4\text{He}$  cryostat equipped with a superconducting solenoid, a helium vapor evacuation system, and a Sharvin membrane manostat for helium vapor pressure stabilization. The temperature stabilization accuracy was no worse than 0.002 K. The magnetic field was applied parallel to the plane of the FSF-sandwich layers along the current flow direction (Fig. 1a).

Series of magnetoresistance curves for different temperatures were measured in the range of  $2.48\text{ K} \leq T \leq 2.55\text{ K}$  near the superconducting transition (Fig. 2a). As an example, Fig. 2b shows the complete magnetoresistance curve at a temperature of 2.48 K, close to the lower edge of the superconducting transition. At high fields, when both F layers are magnetized to saturation, the resistance does not depend on the history: black and red branches in Fig. 2b, corresponding to opposite sweep directions, almost coincide at  $|H| \approx 20\text{--}30\text{ Oe}$ . The increase in the resistance in this field range qualitatively corresponds to the quadratic suppression law of the superconducting order parameter for a thin film in a parallel magnetic field according to the Ginzburg–Landau theory [26] (see the dotted line in Fig. 2b). The change in the magnetoresistance in the range  $|H| < 20\text{ Oe}$  is in agreement with the measurements of the magnetization reversal curves  $M(H)$  of separate  $\text{Pd}_{0.99}\text{Fe}_{0.01}$  layers with similar thicknesses (25 and 40 nm) [25]. When  $H$  varies from  $-10\text{ Oe}$  to  $0\text{ Oe}$ , the initially negative magnetization of the 25-nm-thick layer decreases in absolute value owing to the disorientation of the magnetic moments of the clusters [27]. Under the same variation of the field  $H$ , the magnetoresistance curve of the FSF microbridge (see the black line in Fig. 2b) goes below the quadratic envelope and then reaches a local minimum at the field  $H = +2.3\text{ Oe}$  corresponding to the

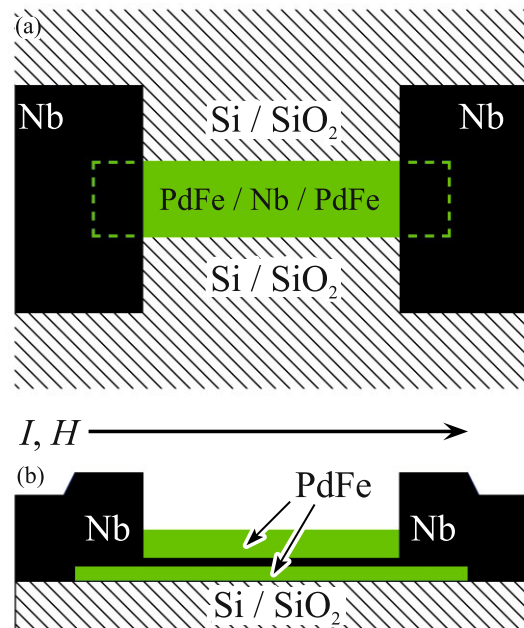


**Fig. 1.** (Color online) (a) Schematic of the  $\text{Pd}_{0.99}\text{Fe}_{0.01}\text{-Nb-Pd}_{0.99}\text{Fe}_{0.01}$  FSF microbridge connecting niobium pads. The arrow shows the direction of the magnetic field and the bias current. (b) Schematic cross section of the same microbridge.

coercive field of the thin F layer in accordance with [25]. The micromagnetic simulation [2] showed that the magnetization reversal of the cluster ferromagnet occurs through the formation of a vortex magnetic state (see also [23]). Therefore, a small increase in the resistance (decrease in the critical temperature) in the range from  $+2.3\text{ Oe}$  to  $+4.8\text{ Oe}$  may be associated with the effect of triplet superconducting correlations [28] caused by the appearance of noncollinear magnetic configurations with respect to the magnetization of the magnetically harder upper F layer. With a further increase in  $H$ , the magnetically softer lower F layer is magnetized in the positive direction with the appearance of an antiparallel state, since the magnetization of the upper F layer remains negative and changes slightly in the field range of  $|H| < 7\text{--}8\text{ Oe}$  according to [25]. Therefore, a drop in the resistance occurs in the field range of  $4.8\text{--}8\text{ Oe}$  due to the direct spin-valve effect [12]. Upon increasing  $H$  above the coercive field of the upper layer (about  $9\text{ Oe}$  according to [25]), the magnetization of the latter also becomes positive and the microbridge goes into the parallel state. Therefore, a sharp increase in the resistance with a gradual return to the quadratic envelope occurs in the field range of  $9\text{--}25\text{ Oe}$ .

We study the possibility of storing the low-resistance state achieved in fields of about  $9\text{ Oe}$  (Fig. 2b). The result is presented in Fig. 2c, which shows a par-

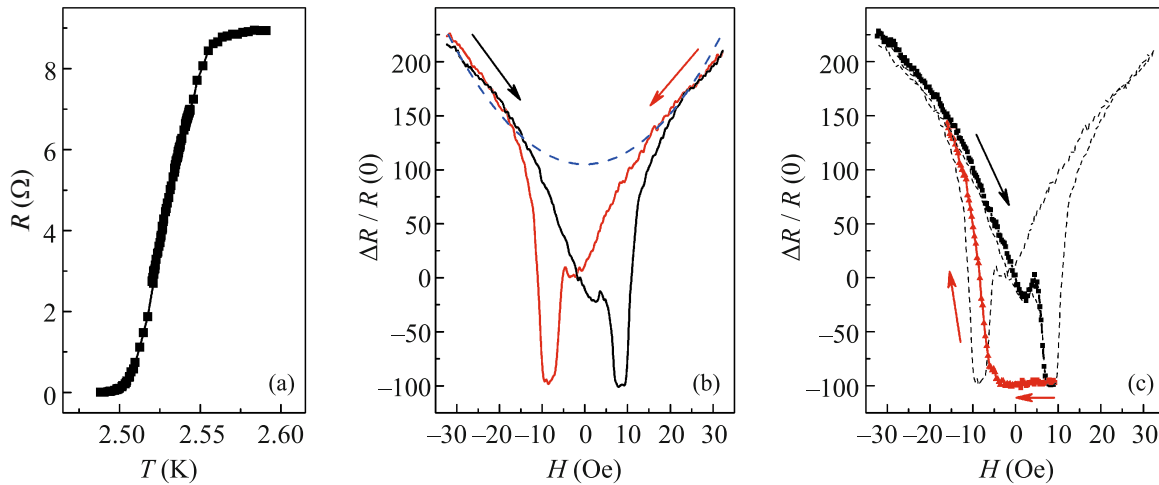


**Fig. 2.** (Color online) (a) Temperature dependence of the resistance of the  $6 \times 20\text{-}\mu\text{m}$   $\text{Pd}_{0.99}\text{Fe}_{0.01}\text{-Nb-Pd}_{0.99}\text{Fe}_{0.01}$  FSF microbridge near the superconducting transition. The thicknesses of the upper and lower F layers are 45 and 22 nm, respectively, and the thickness of the superconducting layer is 13 nm. (b) Magnetoresistance curves for the same microbridge at a temperature of 2.48 K. The arrows show the direction of the magnetic field sweep. The dashed line schematically shows the parabolic envelope of the magnetoresistance curve (see discussion in the main text). (c) Partial magnetoresistance loop of the same microbridge at the same temperature (see discussion in the main text). The arrows show the direction of the magnetic field sweep. The dashed line shows the complete magnetoresistance loop shown in panel (b). The bias current is  $20\ \mu\text{A}$ .

tial magnetoresistance curve of the studied microbridge. The initial state of the sample corresponded to a large negative magnetic field ( $-32\ \text{Oe}$ ), in which both layers were magnetized to saturation in the negative direction. When the field was swept in the positive direction, the minimum of the negative magnetoresistance peak was reached in the field of  $+9\ \text{Oe}$  (black line). At this point, the direction of the magnetic field sweep was reversed (red line). It can be seen that the low-resistance state is retained in this case down to  $-5\ \text{Oe}$ . With a further increase in the magnitude of the negative magnetic field, the magnetoresistance returns gradually to the initial section of the loop (in fields from  $-15$  to  $-20\ \text{Oe}$ ). Such a process can be carried out in a cyclic manner, thereby switching the sample from a high- to a low-resistance state and vice versa.

For practical applications, it is important that both low- and high-resistance states are stable. This allows the use of the FSF microbridge as a superconducting memory element. Figure 3a shows that a pulse with an amplitude of  $-16\ \text{Oe}$  is sufficient to switch the sample into a magnetized (high-resistance) state with a high voltage level. It is reasonable to denote this state as the digital state 1. The application of an opposite pulse with an amplitude of  $+9\ \text{Oe}$  should switch the sample to the low-resistance state 0 with a low voltage. Figure 3b shows that the sequential application of such pulses results in a reproducible switching of the implemented memory element between states 0 and 1. According to Fig. 3b, the stability of the digital states is observed at times of at least several tens of seconds.

The operating temperature of the studied memory element corresponds to the lower edge of the supercon-

ducting transition (Fig. 2a), which is determined by the influence of the  $\text{Pd}_{0.99}\text{Fe}_{0.01}$  F layers on the superconducting order parameter in the niobium S layer. Until recently, the proximity effect in  $\text{Nb/Pd}_{0.99}\text{Fe}_{0.01}$  bilayers was studied insufficiently. In the only experimental work [29], the dependence of the critical temperature on the ferromagnet thickness for unstructured  $\text{Nb-Pd}_{1-x}\text{Fe}_x\text{-Nb}$  samples is given for seven different iron concentrations ranging from 0 to 100%. The thickness of the  $\text{Pd}_{1-x}\text{Fe}_x$  layer for all compositions varied in the range of 0–10 nm. The nonmonotonic dependence of the critical temperature  $T_c(d_F)$  was observed for concentrations of 13 and 20%. For the  $\text{Pd}_{0.99}\text{Fe}_{0.01}$  alloy, such an effect was not observed earlier (as well as in this work): the critical temperature of the samples decreased monotonically with increasing thickness of the F layer. This result is in agreement with the cluster nature of magnetism in  $\text{Pd}_{0.99}\text{Fe}_{0.01}$  presented in [25, 30, 31]. According to it, thin-film layers of such an alloy can be represented as a set of 10-nm magnetic clusters with an intercluster distance of about 100 nm. Therefore, the films with thickness less than  $d_0 = 10\ \text{nm}$  are nonmagnetic. In fact, the approximation of the  $T_{\text{Curie}}(d_{\text{PdFe}})$  dependence presented in our work [19] gives a threshold thickness of 5–10 nm.<sup>1</sup> The increase in the thickness of the  $\text{Pd}_{0.99}\text{Fe}_{0.01}$  film above 10 nm (at least up to about 200 nm) leads to a monotonic increase in the Curie temperature. This is the

<sup>1</sup> Below, the threshold thickness  $d_0$  is taken as 10 nm for certainty. In this work, the  $\text{Pd}_{0.99}\text{Fe}_{0.01}$  films can be considered as nonmagnetic because their Curie temperature is below the operating temperature of the sample.

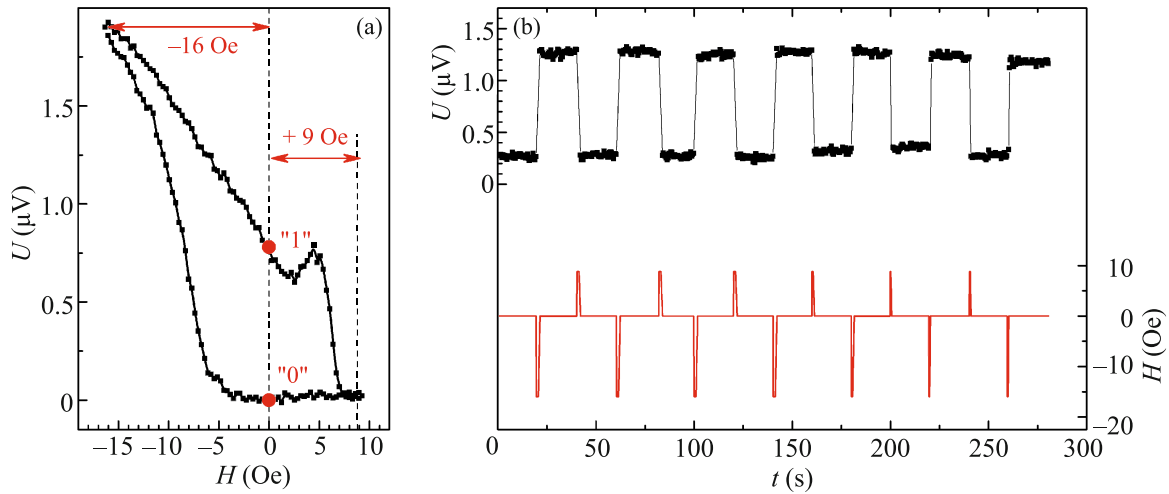


**Fig. 3.** (Color online) (a) Magnetic field dependence of the voltage across the FSF microbridge obtained at a bias current of  $20 \mu\text{A}$  and a temperature of  $2.48 \text{ K}$ . The arrows indicate the amplitudes of the pulses used to switch digital states in Fig. 3b. The digital states 0 and 1 are schematically marked by red circles. (b) Time dependence of (top line) the voltage across the FSF microbridge illustrating its switching between two digital states under the action of (bottom line) a sequence of magnetic field pulses at a temperature of  $T = 2.50 \text{ K}$  and a bias current of  $15 \mu\text{A}$ .

thickness range ( $d_{\text{PdFe}} > 10 \text{ nm}$ ) that is practically important for the use of the  $\text{Pd}_{0.99}\text{Fe}_{0.01}$  alloy as a weak ferromagnet in the devices under discussion. In this work, we study the  $T_c(d_{\text{PdFe}})$  dependence for Nb– $\text{Pd}_{0.99}\text{Fe}_{0.01}$  bilayer samples in a wide range of thicknesses of the F layer up to  $d_{\text{PdFe}} = 75 \text{ nm}$ , which is approximately two times higher than the maximum thickness of the F layer, which we used in the previously studied elements of the Josephson magnetic memory [19].

To fabricate FS bilayers, the wedge method was applied (see, e.g., [32]), in which the thickness of the superconducting layer (see Fig. 4b) was approximately constant all over the long substrate (60 mm in length), and the thickness of the ferromagnet at the thick and thin ends differed by a factor of about 4 (see Fig. 4c). The technological parameters of the thin film deposition process were similar to those given in [1]. To study the wide range of F layer thicknesses (0–75 nm), three FS wedges were fabricated covering different parts of this range. The chosen thickness of the niobium layer  $d_S \approx 11 \text{ nm}$  is rather large compared to the niobium superconducting coherence length of  $\xi_S \approx 7 \text{ nm}$  [5]. In this work, the increased thickness of the S layer provided a fairly high critical temperature for all samples, which can be experimentally measured using a  $^4\text{He}$  cryostat, up to maximum thicknesses of the  $\text{Pd}_{0.99}\text{Fe}_{0.01}$  layer. Each FS wedge was cut across the long side into the experimentally studied stripes 2 mm in width. The thickness of the  $\text{Pd}_{0.99}\text{Fe}_{0.01}$  layer was determined on the basis of a previously studied profile (see Fig. 4c). The results of the performed experiments are presented in Fig. 4a. In the thickness range of  $0 < d_{\text{PdFe}} < 7 \text{ nm}$ , the critical temperature  $T_c$  of the

bilayer decreases sharply from  $7.0$  to  $4.2 \text{ K}$ . In the  $d_{\text{PdFe}}$  range of  $7\text{--}10 \text{ nm}$ , the critical temperature is almost constant. In the practically important  $d_{\text{PdFe}}$  range of  $10\text{--}75 \text{ nm}$ , the critical temperature decreases by  $2 \text{ K}$  more in a linear manner on average. Wavelike deviations of the experimental points are most likely associated with a spatial change in the thickness of the superconducting layer along the wedge within  $0.4 \text{ nm}$  (about  $3.5\%$  with respect to the average value of  $11.2 \text{ nm}$ )<sup>2</sup> as shown in Fig. 4b.

An unexpected result of the experiment presented in Fig. 4a is the decrease in  $T_c$  in a very wide range of thicknesses (up to  $75 \text{ nm}$ ). In previous experiments (see, e.g., [3–5, 23]), a significant change in the critical temperature of FS bilayers was observed only at sufficiently small F layer thicknesses (less than  $10 \text{ nm}$ ), which was due to a small depth of the Cooper pair penetration into a ferromagnet  $\xi_{\text{F1}}$  (see the definition in [33]). For example, the  $\xi_{\text{F1}}$  value in a weakly ferromagnetic  $\text{Cu}_{0.47}\text{Ni}_{0.53}$  alloy is only  $1.3 \text{ nm}$  [33]. Note that the critical temperature in our case (in the “non-magnetic” range of thicknesses  $d_{\text{PdFe}} < 10 \text{ nm}$ ) also decreases abruptly with a plateau in the range of  $7 \text{ nm} < d_{\text{PdFe}} < 10 \text{ nm}$  (see Fig. 4a). This indicates the smallness of even the “normal” (“thermal”) coherence length for our thin-film  $\text{Pd}_{0.99}\text{Fe}_{0.01}$  layers  $\xi_{\text{PdFe}} = \sqrt{\hbar D_{\text{PdFe}}/2\pi k T_c}$ , where  $D_{\text{PdFe}}$  is the diffusion coefficient of electrons. A further decrease in  $T_c$  of bilayers in the range of  $10 \text{ nm} < d_{\text{PdFe}} < 75 \text{ nm}$  is most likely due to the previously noted [19, 27] enhancement of ferro-

<sup>2</sup> The spatial distribution of the niobium layer thickness was measured with a Talystep profilometer (Taylor Hobson) using a special sample made with ten deposition rotations.

magnetism in the  $\text{Pd}_{0.99}\text{Fe}_{0.01}$  layer caused by an increase in the intercluster exchange interaction with increasing  $d_{\text{PdFe}}$ .

To test this hypothesis, numerical simulations were performed by solving the equations of the microscopic theory developed for hybrid  $\text{Pd}_{0.99}\text{Fe}_{0.01}\text{FS}$  structures in [21, 34]. The result is presented by the solid line in Fig. 4a. It is seen that satisfactory agreement with the experiment can be obtained even with a linear dependence of the exchange energy  $E_{\text{ex}}$  in the  $\text{Pd}_{0.99}\text{Fe}_{0.01}$  layer on its thickness at  $d_{\text{PdFe}} > d_0$ :

$$E_{\text{ex}}(d_{\text{PdFe}})/k_B = \alpha(d_{\text{PdFe}} - d_0)$$

(see the inset in Fig. 4a). The fitting parameters were the transparencies of the FS interface  $\gamma \approx 0.35$  and  $\gamma_{\text{BFS}} \approx 0.2$  (see the definition in [21]), the characteristic length  $\xi^* = \sqrt{\hbar D_{\text{PdFe}}/2\pi k T_c(0)} = 0.44\xi_S$ , and the phenomenological parameter  $\alpha = 1.26 \text{ K/nm}$  characterizing the rate of increase in the exchange energy with the thickness of the  $\text{Pd}_{0.99}\text{Fe}_{0.01}$  layer. Here,  $T_c(0) = 7.0 \text{ K}$  is the critical temperature of a single niobium layer<sup>3</sup> with a thickness of  $d_S \approx 11 \text{ nm}$ , and  $\xi_S \approx 6.68 \text{ nm}$  is the coherence length in the niobium S layer according to [5]. The characteristic spatial scale  $\xi^* \approx 2.9 \text{ nm}$  corresponds to the minimum of the thermal coherence length  $\xi_{\text{PdFe}}$  for the  $\text{Pd}_{0.99}\text{Fe}_{0.01}$  layer in the nonmagnetic range ( $d_{\text{PdFe}} < 10 \text{ nm}$ ). At large thicknesses ( $d_{\text{PdFe}} > 10 \text{ nm}$ ),  $\xi^*$  is a parameter of the microscopic theory and has no explicit physical meaning<sup>4</sup> since the coherence length in the ferromagnetic layer is determined by the effective exchange interaction energy  $E_{\text{ex}}$  and, possibly, by other depairing processes [33]. The exchange energy  $E_{\text{ex}}$  in temperature units increases to 80 K (see the inset of Fig. 4a), which qualitatively corresponds to a change in the Curie temperature of single  $\text{Pd}_{0.99}\text{Fe}_{0.01}$  layers according to [19]. A more detailed analysis of the  $T_c(d_{\text{PdFe}})$  dependence for Nb– $\text{Pd}_{0.99}\text{Fe}_{0.01}$  FS bilayers, taking into account the refined material parameters and the nonuniform profile of the superconducting film, will be presented in our future publications.

Returning to the practical result of the research performed, it can be noted that a superconducting logic element with the voltage distinction  $\Delta U$  of about  $1 \mu\text{V}$  between logic states 0 and 1 was implemented (Fig. 3b). This value corresponds to the characteristic Josephson frequency  $f_c = \Delta U/\Phi_0$  of about  $0.5 \text{ GHz}$  ( $\Phi_0$  is the magnetic flux quantum). The inverse value  $1/f_c \approx 2 \text{ ns}$  determines the readout time of the digital state [20] when using such memory elements in rapid single-flux quantum (RSFQ) logic devices [22]. The

<sup>3</sup> See the point  $d_F = 0$  in Fig. 4a.

<sup>4</sup> In fact, the parameter  $\xi^*$  characterizes the diffusive motion of electrons in the  $\text{Pd}_{0.99}\text{Fe}_{0.01}$  layer over the entire range of thicknesses within the microscopic theory [21, 34].

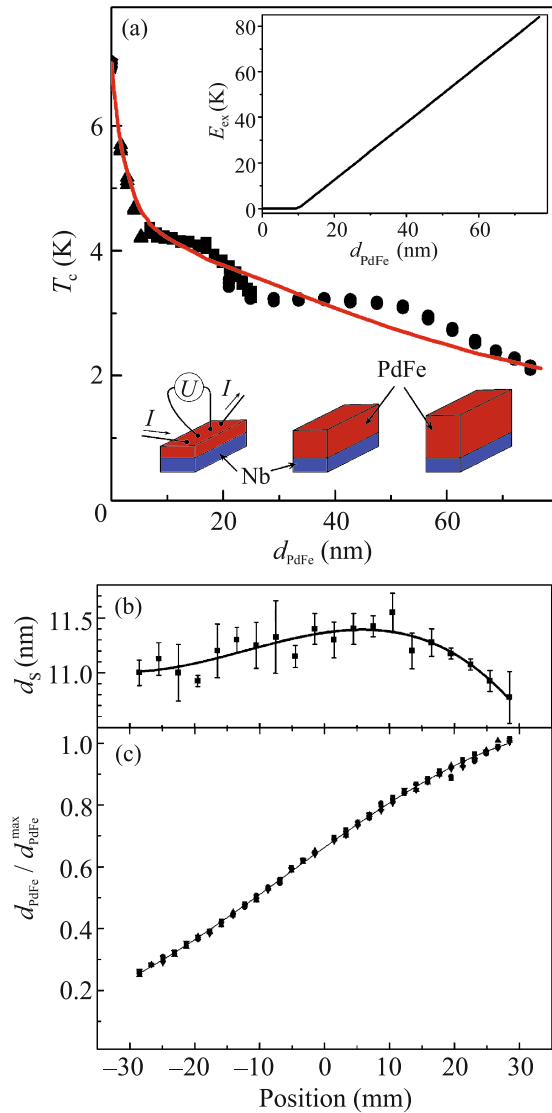


**Fig. 4.** (Color online) (a) Critical temperature of Nb– $\text{Pd}_{0.99}\text{Fe}_{0.01}$  FS bilayers versus the thickness of the ferromagnet layer at a superconductor thickness of about 11 nm. Points of different shapes correspond to three different FS bilayers fabricated using the wedge deposition method. The data for the beginning, middle, and end of the superconducting transition are given. The red line shows the approximation of the experimental data based on the microscopic theory (see discussion in the main text). The inset shows the exchange energy (exchange field) versus the thickness of the ferromagnet, which was used in the calculation shown by the red line. (b, c) Thicknesses of niobium,  $d_S$ , and  $\text{Pd}_{0.99}\text{Fe}_{0.01}$ ,  $d_{\text{PdFe}}$ , layers versus the position on the substrate. The profile of the  $\text{Pd}_{0.99}\text{Fe}_{0.01}$  layer (see panel (c)) is normalized to its maximum thickness in the corresponding FS bilayer.

characteristic frequency obtained is close to the lower frequency limit of RSFQ circuits, which makes it possible, in principle, to rely on the practical use of  $\text{Pd}_{0.99}\text{Fe}_{0.01}$ –Nb– $\text{Pd}_{0.99}\text{Fe}_{0.01}$  bridges in digital super-

conducting electronics. The power consumption in the resistive state is about 15 pW, which is 3000 times less than that obtained in our previous work [2] and 2–4 orders of magnitude less than the power consumption of CMOS memory elements discussed recently in [35, 36]. However, the operating speed of the presented element is still not high enough for wide use in the entire frequency range of RSFQ devices. Therefore, studies aimed at increasing the voltage distinction of the memory element based on  $\text{Pd}_{0.99}\text{Fe}_{0.01}$ – $\text{Nb}$ – $\text{Pd}_{0.99}\text{Fe}_{0.01}$  structures will continue. The subject of future research is, first of all, the nature of the low-resistance state, as well as the possibility of using multilayer  $\text{Pd}_{0.99}\text{Fe}_{0.01}$ – $\text{Nb}$ – $\text{Pd}_{0.99}\text{Fe}_{0.01}$  FSF structures as a Josephson barrier in multilayer sandwich junctions [37].

Thus, in the present work, we have studied the negative magnetoresistance effect in the FSF microbridge consisting of superconducting niobium and a weakly ferromagnetic  $\text{Pd}_{0.99}\text{Fe}_{0.01}$  alloy. The effect of storing the low-resistance state of the bridge has been found. Its operation as a memory element switched by pulses of an external magnetic field has been demonstrated. The dependence of the critical temperature of the  $\text{Nb}$ – $\text{Pd}_{0.99}\text{Fe}_{0.01}$  FS bilayer structures on the thickness of the ferromagnet in an unexpectedly wide range of thicknesses has been revealed. It has been shown that this phenomenon can be described using a microscopic theory that takes into account the enhancement of the exchange interaction with increasing thickness of the  $\text{Pd}_{0.99}\text{Fe}_{0.01}$  layer.

#### ACKNOWLEDGMENTS

We are grateful to V.N. Shilov and N.S. Stepanov for their help in preparing the samples and performing the experiments.

#### FUNDING

Fabrication of samples and experimental studies were supported by the Russian Foundation for Basic Research (project nos. 20-02-00864 and 19-32-90162, respectively). The development of the fabrication technology, including the fabrication of photomasks, the implementation of the wedge method, etc., was supported by the Ministry of Science and Higher Education of the Russian Federation (project no. 0718-2020-0025). Numerical simulation was supported by the Ministry of Science and Higher Education of the Russian Federation (project no. 075-15-2021-1353).

#### CONFLICT OF INTEREST

The authors declare that they have no conflicts of interest.

#### OPEN ACCESS

This article is licensed under a Creative Commons Attribution 4.0 International License, which permits use, sharing,

adaptation, distribution and reproduction in any medium or format, as long as you give appropriate credit to the original author(s) and the source, provide a link to the Creative Commons license, and indicate if changes were made. The images or other third party material in this article are included in the article's Creative Commons license, unless indicated otherwise in a credit line to the material. If material is not included in the article's Creative Commons license and your intended use is not permitted by statutory regulation or exceeds the permitted use, you will need to obtain permission directly from the copyright holder. To view a copy of this license, visit <http://creativecommons.org/licenses/by/4.0/>.

#### REFERENCES

1. L. N. Karelina, V. V. Bol'ginov, Sh. A. Erkenov, S. V. Egorov, I. A. Golovchanskii, V. I. Chichkov, A. Ben Hamida, and V. V. Ryazanov, *JETP Lett.* **112**, 705 (2020).
2. L. N. Karelina, R. A. Hovhannisyan, I. A. Golovchanskii, V. I. Chichkov, A. Ben Hamida, V. S. Stolyarov, L. S. Uspenskaya, Sh. A. Erkenov, V. V. Bolginov, and V. V. Ryazanov, *J. Appl. Phys.* **130**, 173901 (2021).
3. V. V. Ryazanov, V. A. Oboznov, A. S. Prokof'ev, and S. V. Dubonos, *JETP Lett.* **77**, 39 (2003).
4. V. Zdravkov, A. Sidorenko, G. Obermeier, S. Gsell, M. Schreck, C. Müller, S. Horn, R. Tidecks, and L. R. Tagirov, *Phys. Rev. Lett.* **97**, 057004 (2006).
5. V. I. Zdravkov, J. Kehrle, G. Obermeier, et al., *Phys. Rev. B* **82**, 054517 (2010).
6. V. I. Zdravkov, J. Kehrle, D. Lenk, G. Obermeier, A. Ullrich, C. Müller, H. A. Krug von Nidda, R. Morari, A. S. Sidorenko, L. R. Tagirov, S. Horn, and R. Tidecks, *J. Appl. Phys.* **114**, 033903 (2013).
7. J. S. Jiang, D. Davidović, D. H. Reich, and C. L. Chien, *Phys. Rev. Lett.* **74**, 314 (1995).
8. T. H. Mühge, N. N. Garif'yanov, Yu. V. Goryunov, G. G. Khaliullin, L. R. Tagirov, K. Westerholt, I. A. Garifullin, and H. Zabel, *Phys. Rev. Lett.* **77**, 1857 (1996).
9. I. A. Garifullin, D. A. Tikhonov, N. N. Garif'yanov, L. Lazar, Yu. V. Goryunov, S. Ya. Khlebnikov, L. R. Tagirov, K. Westerholt, and H. Zabel, *Phys. Rev. B* **66**, 0205051(R) (2002).
10. J. Y. Gu, C.-Y. You, J. S. Jiang, J. Pearson, Ya. B. Bazaliy, and S. D. Bader, *Phys. Rev. Lett.* **89**, 267001 (2002).
11. A. I. Buzdin, *Rev. Mod. Phys.* **77**, 935 (2005).
12. L. R. Tagirov, *Phys. Rev. Lett.* **83**, 2058 (1999).
13. A. I. Buzdin, A. V. Vedyayev, and N. V. Ryzhanova, *Europhys. Lett.* **48**, 686 (1999).
14. P. V. Leksin, N. N. Garif'yanov, I. A. Garifullin, J. Schumann, H. Vinzelberg, V. Kataev, O. G. Schmidt, and B. Büchner, *Appl. Phys. Lett.* **97**, 102505 (2010).
15. V. N. Kushnir, A. S. Sidorenko, L. R. Tagirov, and M. Yu. Kupriyanov, in *Functional Nanostructures and Metamaterials for Superconducting Spintronics* (Cham, Springer, 2018), Sect. 1, p. 1.
16. L. R. Tagirov, M. Yu. Kupriyanov, V. N. Kushnir, and A. S. Sidorenko, in *Functional Nanostructures and*

- Metamaterials for Superconducting Spintronics* (Cham, Springer, 2018), Sect. 2, p. 31.
17. A. Singh, S. Voltan, K. Lahabi, and J. Aarts, *Phys. Rev. X* **5**, 021019 (2015).
  18. S. Voltan, A. Singh, and J. Aarts, *Phys. Rev. B* **94**, 054503 (2016).
  19. V. V. Bol'ginov, V. S. Stolyarov, D. S. Sobanin, A. L. Karpovich, and V. V. Ryazanov, *JETP Lett.* **95**, 366 (2012).
  20. T. I. Larkin, V. V. Bol'ginov, V. S. Stolyarov, V. V. Ryazanov, I. V. Vernik, S. K. Tolpygo, and O. A. Mukhanov, *Appl. Phys. Lett.* **100**, 222601 (2012).
  21. S. V. Bakurskiy, N. V. Klenov, I. I. Soloviev, V. V. Bol'ginov, V. V. Ryazanov, I. V. Vernik, O. A. Mukhanov, M. Yu. Kupriyanov, and A. A. Golubov, *Appl. Phys. Lett.* **102**, 192603 (2013).
  22. K. K. Likharev and V. K. Semenov, *IEEE Trans. Appl. Supercond.* **1**, 3 (1991).
  23. I. A. Golovchanskiy, V. V. Bolginov, V. S. Stolyarov, N. N. Abramov, A. Ben Hamida, O. V. Emelyanova, B. S. Stoyarov, M. Yu. Kupriyanov, A. A. Golubov, and V. V. Ryazanov, *Phys. Rev. B* **94**, 214514 (2016).
  24. I. I. Soloviev, S. V. Bakurskiy, V. I. Ruzhickiy, N. V. Klenov, M. Yu. Kupriyanov, A. A. Golubov, O. V. Skryabina, and V. S. Stolyarov, *Phys. Rev. Appl.* **16**, 044060 (2021).
  25. L. S. Uspenskaya and I. N. Khlyustikov, *J. Exp. Theor. Phys.* **125**, 875 (2017).
  26. V. V. Schmidt, *Introduction to Superconductor Physics* (MTsNMO, Moscow, 2000), Chap. 3, p. 17 [in Russian].
  27. L. S. Uspenskaya, A. L. Rakhmanov, L. A. Dorosinskii, A. A. Chugunov, V. S. Stolyarov, O. V. Skryabina, and S. V. Egorov, *JETP Lett.* **97**, 155 (2013).
  28. F. Bergeret, A. Volkov, and K. Efetov, *Rev. Mod. Phys.* **77**, 1321 (2005).
  29. M. Schöck, C. Sürgers, and H. von Löhneysen, *Eur. Phys. J. B* **14**, 1 (2000).
  30. L. S. Uspenskaya, A. L. Rakhmanov, L. A. Dorosinskii, S. I. Bozhko, V. S. Stolyarov, and V. V. Bolginov, *Mater. Res. Express* **1**, 036104 (2014).
  31. I. A. Golovchanskiy, V. V. Bolginov, N. N. Abramov, V. S. Stolyarov, A. Ben Hamida, V. I. Chichkov, D. Roditchev, and V. V. Ryazanov, *J. Appl. Phys.* **120**, 163902 (2016).
  32. A. S. Sidorenko, V. I. Zdravkov, A. A. Prepelitsa, C. Helbig, Y. Luo, S. Gsell, M. Schreck, S. Klimm, S. Horn, L. R. Tagirov, and R. Tidecks, *Ann. Phys.* **12**, 37 (2003).
  33. V. A. Oboznov, V. V. Bol'ginov, A. K. Feofanov, V. V. Ryazanov, and A. I. Buzdin, *Phys. Rev. Lett.* **96**, 197003 (2006).
  34. S. V. Bakurskiy, N. V. Klenov, I. I. Soloviev, N. G. Pugach, M. Yu. Kupriyanov, and A. A. Golubov, *Appl. Phys. Lett.* **113**, 082602 (2018).
  35. C. C. Wang and C. P. Kuo, in *Proceedings of the IEEE International Symposium on Circuits and Systems* (2021), p. 1.  
<https://doi.org/10.1109/ISCAS51556.2021.9401099>
  36. A. K. Mishra, U. Chopra, and D. Vaithyanathan, *IEEE Trans. Circuits Syst. II: Express Briefs* **69**, 1592 (2022).
  37. N. V. Klenov, Yu. N. Khaydukov, S. V. Bakurskiy, R. Morari, I. Soloviev, V. Boian, Th. Keller, M. Yu. Kupriyanov, A. Sidorenko, and B. Keimer, *Beilstein J. Nanotechnol.* **10**, 833 (2019).

*Translated by L. Mosina*